Journal of Alloys and Compounds 615 (2014) S621–S626

Contents lists available at ScienceDirect

Journal of Alloys and Compounds

journal homepage: www.elsevier.com/locate/jalcom

The use of Nb in rapid solidified Al alloys and composites

F. Audebert [a,b,c,*], M. Galano [b], F. Saporiti [a]

[a] Advanced Materials Group, Facultad de Ingeniería, Universidad de Buenos Aires, Paseo Colón 850, Ciudad de Buenos Aires 1063, Argentina
[b] Department of Materials, University of Oxford, Parks Road, OX1 3PH Oxford, UK
[c] Department of Mechanical Engineering and Mathematical Sciences, Oxford Brookes University, Wheatley Campus, OX33 1HX Oxford, UK

ARTICLE INFO

Article history:
Available online 23 December 2013

Keywords:
Niobium
Aluminium alloys
Rapid solidification
Amorphous
Quasicrystals
Composites

ABSTRACT

The worldwide requirements for reducing the energy consumption and pollution have increased the demand of new and high performance lightweight materials. The development of nanostructured Al-based alloys and composites is a key direction towards solving this demand. High energy prices and decreased availability of some alloying elements open up the opportunity to use non-conventional elements in Al alloys and composites. In this work the application of Nb in rapid solidified Al-based alloys and Al alloys matrix composites is reviewed. New results that clarify the effect of Nb on rapid solidified Al alloys and composites are also presented. It is observed that Nb stabilises the icosahedral Al–Fe/Cr clusters, enhances the glass forming ability and shifts the icosahedral phase decomposition towards higher temperatures. Nb provides higher corrosion resistance with respect to the pure Al and Al–Fe–RE (RE: rare earth) alloys in the amorphous and crystalline states. The use of Nb as a reinforcement to produce new Al alloy matrix composites is explored. It is observed that Nb provides higher strength, ductility and toughness to the nanoquasicrystalline matrix composite. Nb appears as a new key element that can improve several properties in rapid solidified Al alloys and composites.

1. Introduction

Aluminum is the second most used metal in the world. Its lightweight and good combination of properties allows it to be used in several industrial sectors. The worldwide requirements for reducing the energy consumption and pollution have increased the demand of new and high performance lightweight materials. The progress in manufacturing technologies and the development of nanomaterials gives the opportunity of exploring the use of new alloying elements and reinforcement particles in composites.

Nb is not a common element used in the commercial Al alloys. However, some reports can be found in the literature of its use as an alloying element in Al alloys and their composites. Three main aims were found for its use: (1) for producing amorphous Al-based alloys [1–7], (2) for producing nanoquasicrystalline Al-based alloys with enhanced stability [8–13], and (3) as reinforcement or alloying component of reinforcement compounds in Al matrix composites [14–16]. In the following sections these three groups of studies are reviewed and new results are presented. In the section corresponding to the amorphous alloys the discussion addresses the role of Nb in the icosahedral clusters in Al–Fe base liquids and the improvement in the corrosion resistance of the rapidly solidified alloys. In the nanoquasicrystalline alloys section the discussion focuses on how Nb improves the stability of the quasicrystalline icosahedral phase. Finally in the section corresponding to the composites new results are reported introducing a new aim for using Nb as a reinforcement phase. Nb particles are added to a high strength nanoquasicrystalline Al alloy to balance the strength, ductility and toughness producing an innovative type of composite.

2. Nb in amorphous Al-based alloys

The first ductile amorphous Al alloys were obtained in 1988 in the systems Al–Fe–Gd and Al-(Y,La)-TM (TM: transition metals) by Shiflet et al. [17] and Inoue et al. [18] respectively. Subsequently, many authors explored several Al-based alloy systems in order to find other ductile amorphous alloys. Years later, Inoue [19] published a review paper that reported several amorphous Al-based alloys produced by rapid solidification. However, there was no mention of any amorphous Al alloy containing Nb. In 1997 Audebert et al. [1] reported the first Al–Fe–Nb alloys containing an amorphous phase. Later, it was found that the partial substitution of Ni by Nb also improves the glass forming ability (GFA) of the Al–Ni-RE (RE: rare earths) alloys [6].

Chemical composition ranges with high GFA in Al alloys systems are normally away from the eutectic composition, as it was described by Bechet and Regazzoni [20]. In particular the Al-rich

* Corresponding author at: Advanced Materials Group, Facultad de Ingeniería, Universidad de Buenos Aires, Paseo Colón 850, Ciudad de Buenos Aires 1063, Argentina.
E-mail addresses: metal@fi.uba.ar, fernando.audebert@materials.ox.ac.uk, faudebert@brookes.ac.uk (F. Audebert).

0925-8388/$ - see front matter © 2013 Elsevier B.V. All rights reserved.
http://dx.doi.org/10.1016/j.jallcom.2013.12.129

corner of the Al–Fe–Nb system has the Al–Fe binary eutectic at 99, 1 at% Al and a peritectic reaction with >99 at%Al for the Al–Nb binary system. The richest Al content intermetallics in those systems are the $Al_{13}Fe_4$ (~76 at%Al) and the Al_3Nb (75 at%Al). The glass forming range (using melt-spinning technique) was determined to be between 90 to 86 at%Al with (Fe/Nb) = 2–4 [1]. This glass forming range is between the eutectic and the stable intermetallic compositions. A similar situation is also observed in the Al–Ni–RE systems [19].

In the Al–Fe system, it is worth noting that the composition of the Al–Fe metastable icosahedral phase (86 at%Al) is within the glass forming range in terms of the Al concentration [21,22]. Moreover, Audebert et al. [2] reported the formation of an icosahedral phase during the crystallization of the Al–Fe–Nb amorphous alloy. Further studies on Al–Fe based amorphous alloys combining X-ray diffraction and Mössbauer spectroscopy led to suggest that the existence of icosahedral clusters in the Al rich alloys of the Al–Fe system would be stabilised by Nb increasing the GFA [7,23]. Therefore, it is reasonable to think that local order of the amorphous Al–Fe and Al–Fe–Nb alloys are very similar. This can be observed by comparing the radial distribution function (RDF) of both amorphous phases. Taking into account that it is not possible to obtain a fully amorphous $Al_{90}Fe_{10}$ (at% here after) sample by melt-spinning, the RDF of this alloy was obtained by molecular dynamic simulation (MDS). The interaction between atoms has been modeled using the potentials developed by Farkas [24] applying the embedded atom method [25]. The simulation was performed following the methodology used in an early work [26]. The RDF corresponding to the $Al_{90}Fe_7Nb_3$ alloy was obtained from the X-ray diffractogram of a melt-spun amorphous sample. Fig. 1 shows the RDFs for both alloys at room temperature. There is an excellent match between both RDFs. Both distributions show a split in the second peak, which would be related to the icosahedral symmetry [26,27]. The minor differences in the RDFs would be related to the slightly larger Nb atomic size (rNb = 146 pm) against the Al atomic size (rAl = 143 pm). The results are a new evidence that strongly suggests that the Nb dissolves in the Al–Fe liquid structure stabilizing an icosahedral local symmetry during the rapid solidification process, which enhances the GFA. This is in agreement with that was suggested in early works [7,23].

In addition to the high hardness values that amorphous Al-based alloys have respect to crystalline Al alloys, probably the most distinctive property of the amorphous phase is the excellent capacity to develop protective oxide layers [19,28]. The first studies found in the literature on corrosion behavior of amorphous Al alloys were the reported by Yoshioka et al. [29] on amorphous Al-TM films produced by physical vapor deposition. An extensive study on the corrosion behavior of several Al-TM binaries and ternaries amorphous films in NaCl and HCl solutions were reported by Hashimoto's group [29]. Probably the earliest reports found on corrosion studies in amorphous Al-based alloys obtained by rapid solidification are the works of Mansour et al. [30,31]. They studied the corrosion behaviour of melt-spun amorphous Al–Fe–Ce alloys in a 0.15 M-NaCl solution. They found that the passive range developed by the amorphous alloys was larger than the one developed by the crystallised samples. The passive layer was formed mainly by $AlO_x(OH)_y$ with minor contents of Fe and Ce. Ce and other rare earths are used successfully for increasing the GFA of the Al-based alloys produced by rapid solidification, thus in the literature the majority of corrosion studies found are on amorphous Al-based alloys containing RE (e.g.: Ce, Gd, La, Y) [32–35]. Only one report on corrosion studies has been found on amorphous Al alloys containing Nb [4]. The authors studied the corrosion behaviour in 1 M-NaCl solution of a melt-spun amorphous $Al_{87}Fe_{10}Nb_3$ alloy. It was observed that the pure Al and the crystallised Al–Fe–Nb samples have a passive range of 250 mV and 400 mV respectively, whereas the alloy in the amorphous state showed a passive range of 2.3 times larger than in the crystalline state and a lower passive current density of $\sim 5 \times 10^{-6}$ A/cm^2.

Unfortunately, the corrosion studies in the literature were carried out using different electrolytes, which makes the comparison among alloys very difficult. Therefore, to compare the effect on the corrosion behaviour when RE or Nb are added to an Al-Fe based alloys two melt-spun amorphous samples with compositions of $Al_{90}Fe_7Nb_3$ and $Al_{90}Fe_5MM_5$ (MM: Mischmetal, RE solid solution with 54 w%Ce and 24 w%La) were prepared. Crystallised samples were prepared by heat treatment in vacuum (10^{-6} mbar) during 1 h at 500 °C. The X-ray diffractograms taken with Cu Kα radiation are shown in Fig. 2a. The amorphous phases show a pre-peak at ~21 and ~19° (2θ, Cu Kα) and a main peak at ~41.5 and ~38° for the Al–Fe–Nb and Al–Fe–MM alloys respectively. The amorphous peaks of the RE containing alloy is shifted towards low angles respect to the one with Nb because of the larger atomic size of the RE atoms (rCe = 181 pm) respect to the Nb atom (rNb = 146 pm). The X-ray diffractograms of the crystallized samples show the stable equilibrium phases, Al, $Al_{13}Fe_4$ and Al_3Nb for the Al–Fe–Nb alloy, and Al, $Al_{11}RE_3$ and the metastable $Al_{10}Fe_2Ce$ phase for the Al–Fe–MM alloy. The potentiodynamic polarization curves obtained at 25 °C in 1 M-NaCl solution deaerated with Ar during 1 h, can be observed in Fig. 2b.

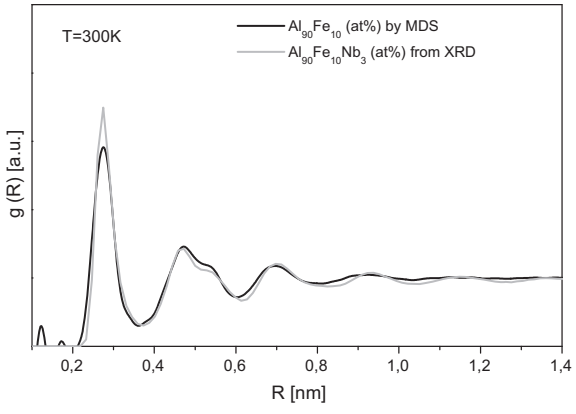

Fig. 1. Radial distribution functions of amorphous alloys, $Al_{90}Fe_{10}$ (at%) obtained by molecular dynamic simulation (MDS); and $Al_{90}Fe_7Nb_3$ (at%) obtained from the X-ray diffractogram (XRD) of a melt-spun sample.

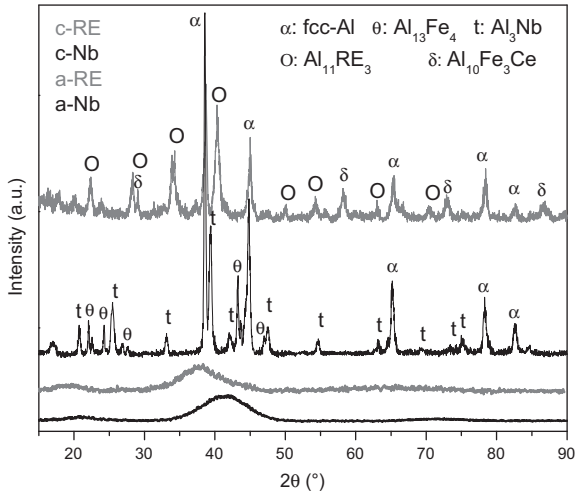

Fig. 2a. X-ray diffractograms of the amorphous (a-) and crystallised (c-) melt-spun samples of $Al_{90}Fe_7Nb_3$ (Nb) and $Al_{90}Fe_5MM_5$ (RE).

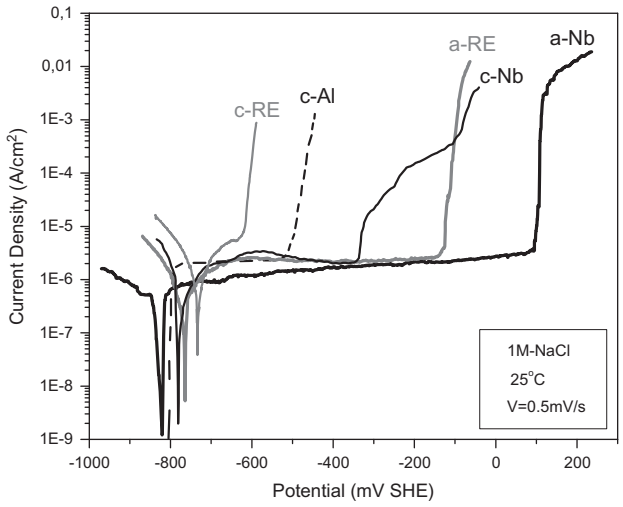

Fig. 2b. Potentiodynamic polarization curves in 1 M-NaCl solution at 25 °C and 0.5 mV/s of the amorphous (a-) and crystallised (c-) melt-spun samples of $Al_{90}Fe_7Nb_3$ (Nb) and $Al_{90}Fe_5MM_5$ (RE). The curve of the crystalline Al (c-Al) was taken from Ref. [36].

Fig. 2b shows that the Al–Fe–Nb alloy, in both amorphous and crystalline states, has a better protective passive layer than the pure crystalline Al. On the contrary, the Al–Fe–MM alloy only has a better behaviour, when is in the amorphous state, than the pure crystalline Al. When the alloys are compared in the crystalline state, it is observed that the addition of Fe and Nb to Al chemically enhances the pitting resistance of the electrochemically formed passive layer. However, the addition of Fe and RE to Al deteriorates the corrosion resistance of the $AlO_x(OH)_y$ passive layer normally formed on pure Al. When both alloys are compared in the amorphous state it is observed that the corrosion resistance of the Al–Fe–Nb is much better than the one for Al–Fe–MM alloy. Having both amorphous alloys similar corrosion potential (∼−800 mV SHE), the Al–Fe–Nb has lower passive current density and shows a higher pitting potential (95 mV SHE) than the Al–Fe–MM (∼−130 mV SHE).

Finally, two important effects of the Nb on Al-based alloys can be observed: (1) Nb increases the GFA in Al–Fe and Al–Ni based alloys, and (2) Nb provides better corrosion resistance in 1 M-NaCl solutions than the REs as alloying elements in Al–Fe based alloys.

3. Nb in nanoquasicrystalline Al-based alloys

Following the conclusions of an early work on the study of the short range order of Al–Fe–X (X: Nb, Sb, RE) melt-spun alloys that predicted that Nb would stabilize the icosahedral symmetry, Galano et al. added Nb to the Al–Fe–Cr based alloys in order to stabilise the quasicrystalline icosahedral phase [8,10,12]. The Nb was added in partial substitution of Fe and Cr modifying the chemical composition of the $Al_{93}(Fe_3Cr_2)_7$ as $Al_{93}Fe_3Cr_2Nb_2$. The alloys were produced by melt-spinning and showed a nanoquascrystalline microstructure composed by nano-icosahedral particles embedded in a fcc-Al matrix. The icosahedral particles were formed by the four elements (Al, Fe, Cr, Nb) confirming that the Nb is dissolved in the icosahedral symmetry. The stabilising effect can be analysed by means of a simple geometrical model that takes into account the space frustration of the icosahedral structure [37,38]

Fig. 3 shows a monatomic icosahedron, where the interatomic distance between two neighboring atoms on the surface is about 5% larger than the distance between the surface atoms and the central atom. Hence, the icosahedron does not consist of regular

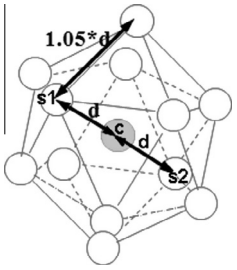

Fig. 3. Monatomic icosahedron and its space frustration.

tetrahedra but of slightly distorted ones. This incompatibility of global filling of space is called "space frustration". When higher shells of the icosahedron are filled up, the gap of packing is continually increased. While the icosahedral structure exhibit the lowest energy at small cluster sizes, when the cluster reaches a critical size due to the increasing space frustration the icosahedral structure becomes disadvantageous compared with fcc or hcp clusters with the same number of atoms. In the case of alloys with small concentrations of alloying elements of smaller or larger sized atoms the space frustration should be reduced increasing the critical cluster size, leading in turn to the stabilisation of the icosahedral clusters. Considering atoms as rigid spheres with the metallic atomic radius and thus considering the aligned atoms s1, c, s2 in Fig. 3 in an Al alloy, if the central site is occupied by a Fe atom the distance "d" would be reduced by 5.94%, if occupied by a Cr atom "d" would be reduced by 5.59%, and if the aligned atoms are: Nb/Fe/Al or Nb/Cr/Al "d" would be reduced by 5.42% and 5.07% respectively.

All the alternatives suggested above reduce the icosahedron space frustration in the order Al–Fe, Al–Cr, Al–Fe–Nb and Al–Cr–Nb. Thus, in an Al–Fe–Cr–Nb alloy that counts with three alloying elements the space frustration could probably be reduced even further increasing the stability of the larger size icosahedral structure, which is in agreement with what has been observed in early experimental works [9,12].

Three melt-spun alloys were produced to observe the predicted stability of the icosahedral phase with alloying elements. Fig. 4a shows the X-ray diffractograms of the melt-spun $Al_{86}Fe_{14}$, $Al_{93}(Fe_3Cr_2)_7$ and $Al_{93}Fe_3Cr_2Nb_2$ alloys. The Al–Fe alloy shows the fcc-Al peaks and non-well formed peaks of the icosahedral or the monoclinic $Al_{13}Fe_4$ phases. Nevertheless, the studies by means of XRD and Mössbauer spectroscopy confirmed that for that composition

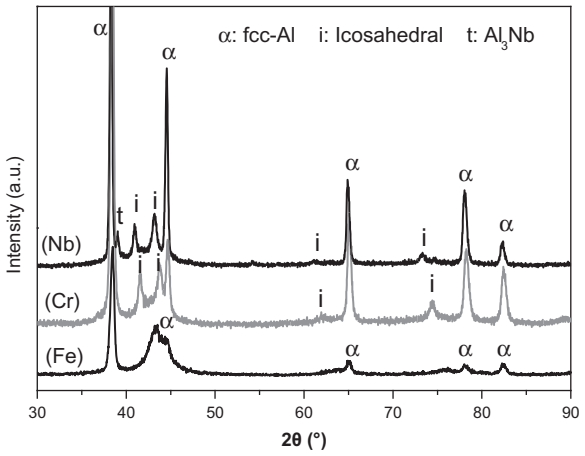

Fig. 4a. X-ray diffractograms of melt-spun samples $Al_{86}Fe_{14}$ (Fe), $Al_{93}(Fe_3Cr_2)_7$ (Cr) and $Al_{93}Fe_3Cr_2Nb_2$ (Nb).

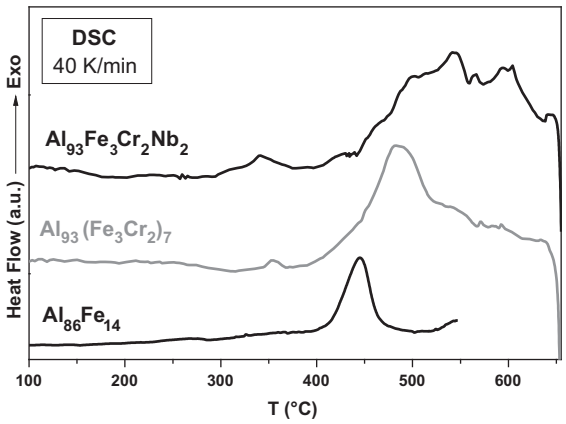

Fig. 4b. DSC curves at 40 K/min of the melt-spun samples $Al_{86}Fe_{14}$, $Al_{93}(Fe_3Cr_2)_7$ and $Al_{93}Fe_3Cr_2Nb_2$.

very small clusters of icosahedral symmetry would be formed [7,21]. The Al–Fe–Cr and the Al–Fe–Cr–Nb alloys show the clear presence of both fcc-Al and icosahedral phases. Differential scanning calorimetric runs were done at 40 K/min under Ar flow in a Pyris 1 Perkin Elmer calorimeter. In Fig. 4b that shows the DSC runs it can be observed that the peak of the icosahedral phase transformation is shifted towards higher temperatures as suggested by the previous icosahedral stability analysis. Moreover, it is observed the transformation peak of the Al–Fe–Cr–Nb is delayed up to the melting of the alloy.

Finally, Nb is observed to stabilise the icosahedral particles in the nanoquasicrystalline Al–Fe–Cr based alloys delaying the icosahedral decomposition towards higher temperatures which contributes to retain the refined microstructure. As a consequence the alloy retains a high strength at higher temperatures [11]. It is worth noting that the large difference in the melting temperature of the alloying elements (Al: 660 °C, Nb: 2469 °C) poses a challenge for a large scale production. However, recently this alloy has been produced by gas atomization and solid bars were extruded successfully [13]. The extruded bars showed high strength at elevated temperature as was previously determined on melt-spun samples [11] which have a great potential for industrial applications.

4. Nb in Al-based alloy matrix composites

Composite materials are manufactured by blending two or more different materials in order to obtain a combination of properties that cannot be reached solely by the alloys or the individual components materials. The progress in engineering and technology in the last decades open up unlimited possibilities for the modern material science and development; materials can be designed, custom-made, depending on their applications. From the point of view of this potential, the metal matrix composites (MMCs) fulfill all the desired design concepts (high stiffness, strength and toughness) for constructional or structural materials. When Al or Al alloys are used as the matrix material the composite (AMC) match the basic requirements of lightweight and strength in automotive, aeronautic and aerospace industries. The common AMCs are composed by a commercial Al matrix reinforced by micron size ceramic particles (SiC, Al_2O_3, TiB_2, etc.). The progress in the manufacturing of nanostructured materials and nanoparticles allowed a new area to be developed; Al based matrix nanocomposites (AMnCs). The nanoparticles normally tend to agglomerate in micron size clusters which makes it difficult to obtain an homogenous distribution in the Al alloy matrix. Other route to produce AMnCs is using a high strength nanostructured Al alloy matrix in combination with softer micron size metallic particles in order to enhance the ductility and toughness without problems of agglomeration and distribution. In the present work micron size Nb particles have been used to improve the toughness of a nanoquasicrystalline Al alloy.

In the literature few reports exist in which Nb is used in composites for structural applications. The majority of them have the aim to produce a very high strength material from two soft metals processed by severe plastic deformation [14,16]. In the present work a different approach is followed. To the best of the authors' knowledge this is the first report in which Nb is used to produce a composite material for enhancing ductility and toughness of a very strong metallic nanostructured Al alloy.

Melt-spun ribbons of $Al_{93}Fe_3Cr_2Ti_2$ alloy were produced in He atmosphere with 20 μm average thickness. The ribbons were chopped in flakes of mm in length and mixed with 10 vol% of pure Nb (99.7%) particles with average size of 100 μm. The alloy powder and the mixed powder were compacted at 375 °C under a pressure of 320 MPa. The billets were extruded at 400 °C with an extrusion ratio of 14. The microstructure of the melt-spun ribbons and the extruded bars were characterized by XRD and scanning electron microscopy. Compression tests on samples of 5 mm diameter and 10 mm in length were carried out at room temperature with an initial strain rate of 10^{-3} S^{-1}.

Fig. 5a shows the microstructure in the longitudinal section of the nanoquasicrystalline extruded bar. The melt-spun flakes compacted and aligned in the extrusion direction (ED) can be observed in addition to the light grey intermetallic precipitates. In Fig. 5b the Nb particles (light grey) can be observed in the longitudinal section of the composite extruded bar. The Nb particles appear slightly deformed in the extrusion direction (ED). Fig. 6a shows the X-ray diffractograms of the melt-spun ribbons and from the cross section of both the alloy and the composite extruded bars. The ribbons were obtained with a microstructure composed of icosahedral particles embedded in a fcc-Al matrix. The diffractograms of the extruded bars show additional peaks corresponding to the Al_3Ti and $Al_{13}Fe_4$ phases which would correspond to the light grey precipitates observed in Fig. 5a. These intermetallics would precipitate during the whole hot processing of compaction plus extrusion.

Complementary, in order to compare the effect of Nb as tough reinforcement in stronger and in softer matrix two additional bars of pure Al powder (63 μm average size) and pure Al with 10 vol%Nb powder were produced.

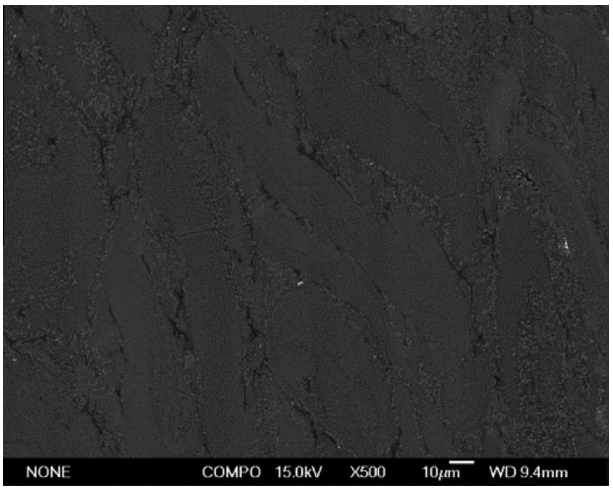

Fig. 5a. Back scattered electron image of the longitudinal section of the nanoquasicrystalline $Al_{93}Fe_3Cr_2Ti_2$ flakes extruded bar.

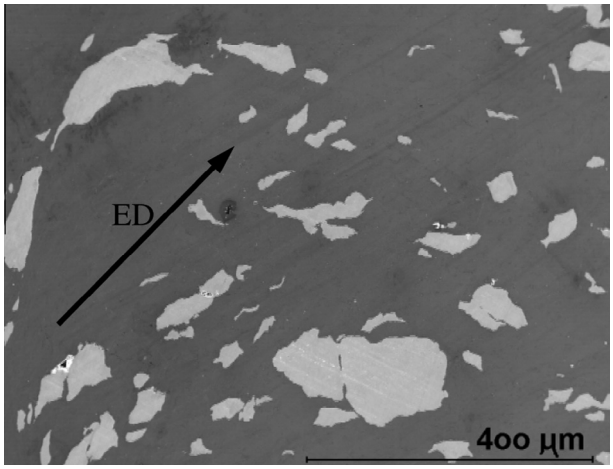

Fig. 5b. Back scattered electron image of the longitudinal section of the composite (10 vol%Nb particles and nanoquasicrystalline $Al_{93}Fe_3Cr_2Ti_2$ flakes) extruded bar. Arrow shows the extrusion direction (ED).

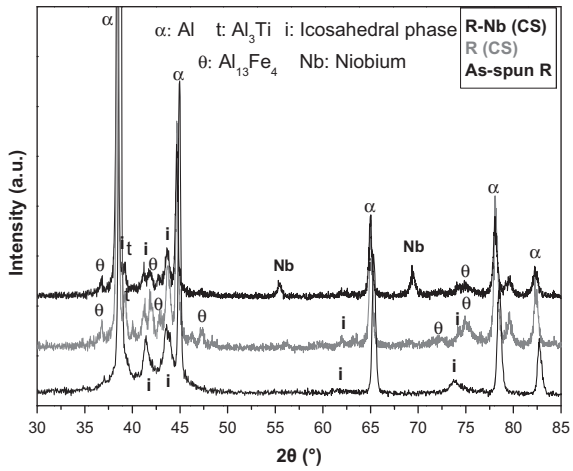

Fig. 6a. X-ray diffractograms of the as-spun $Al_{93}Fe_3Cr_2Ti_2$ ribbon (as-spun R), the cross section of the alloy extruded bar (R(CS)) and the composite extruded bar (R–Nb (CS)).

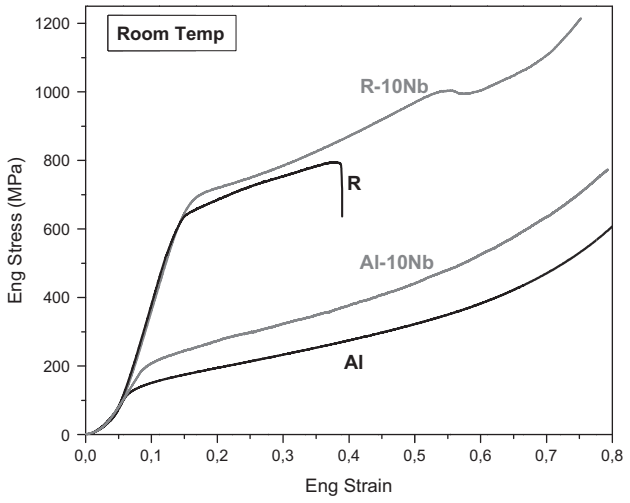

Fig. 6b. Engineering stress–strain compressive curves at room temperature of extruded bars of pure Al powder (Al), nanoquasicrystalline $Al_{93}Fe_3Cr_2Ti_2$ flakes (R) and the composites contained 10 vol%Nb (Al–10Nb and R–10Nb).

Fig. 6b shows the compressive tests of the four extruded bars. It is observed that both composites, having either a softer matrix or a stronger matrix than the reinforcement metallic particles (Nb), have higher compressive Yield stress and high ductility providing higher toughness to the composites. In the case of the Al matrix, the composite shows also higher strain hardening than the pure Al, which is reasonable in view that Nb is a bcc metal which normally has higher strain hardening than the fcc metals. It is worth noting that in the composite with the nanoquasicrystalline matrix Nb particles provide higher ductility transforming the high strength nanoquasicrystalline alloy in a strong and tough composite material. The higher ductility achieved for this composite can be explained by the better plastic behavior of the pure metal (Nb) particles than that of the nanoquasicrystalline alloy matrix. This feature is very important for designing materials for applications in machines and vehicles parts that work in very extreme conditions and demand high security against catastrophic fractures.

5. Summary

The literature on the use of Nb in rapidly solidified Al alloys has been reviewed and key experiments and simulations were performed in order to clarify the effect of Nb in two types of Al alloys, amorphous and nanoquasicrystalline.

The comparison between the radial distribution functions obtained experimentally for an Al–Fe–Nb alloy and the one obtained by molecular dynamic simulation of an Al–Fe alloy strongly suggests and confirms previous evidences that the Nb is dissolved in the icosahedral Al–Fe clusters in the liquid state and retained at room temperature by rapid solidification.

The Nb is found to improve the glass forming ability of rapidly solidified Al–Fe and Al–Ni based alloys. The Al alloys containing Nb show higher corrosion resistance in 1 M-NaCl in amorphous and crystalline state than, at least, the pure Al and Al–Fe–RE alloys.

On the basis of a very simple icosahedron space frustration analysis it is predicted that the addition of small fractions of Nb and Fe (and/or Cr) to the Al contributes to stabilise the icosahedral symmetry from the liquid state. Icosahedral quasicrystalline particles can be formed and retained at room temperature with high stability. When Nb is added in substitution of Fe and Cr the icosahedral decomposition shifts towards higher temperatures, allowing preserving a very refined microstructure at higher temperatures. This fact leads to obtain a new nanostructured Al alloy which retains a high strength in a temperature range of (250–450 °C) where the conventional Al alloys have poor properties.

Nb can be used to produce Al matrix composites. In the literature it was used to produce high strength metal–metal composites by severe plastic deformation. Furthermore, it was proved that Nb can be used to enhance strength, ductility and toughness of very strong nanostructured Al alloys that cannot support severe plastic deformation processes. These new composites can be manufactured by a simple process of hot extrusion of mixed powders.

Finally, Nb appears as a new key element that can improve several properties in rapidly solidified Al alloys and composites.

Acknowledgements

This work was financially supported by UBACyT 2010/058 and PICT-Oxford 2010/2831. Dr. M. Galano thanks the RAEng for their support in research and F. Audebert thanks CONICET. The authors thank CBMM and ALPOCO for providing the Nb and Al powders respectively.

References

[1] F. Audebert, A. García Escorial, H. Sirkin, Scripta Mater. 36-4 (1997) 405–410.
[2] F. Audebert, H. Sirkin, A. García Escorial, Philos. Mag. B 76-4 (1997) 483–487.

[3] F. Audebert, H. Sirkin, A. García Escorial, Non-crystalline and Nanoscale Materials, in: J. Rivas, M.A. López-Quintela (Eds.), Proc. of the V Int. Workshop on Non-Cryst. Solids, World Scientific Publishing Singapore Co., 1998, pp. 367–372.
[4] F. Audebert, S.M. Vázquez, A. Gutierrez, I. Vergara, G. Alvarez, A. García Escorial, H. Sirkin, Mater. Sci. Forum 269 (1998) 837–842.
[5] E. Illekova, D. Janickovic, P. Kubecka, P. Svec, J.C. Gachon, Mater. Sci. Eng. A-375-377 (2004) 946–950.
[6] F. Audebert, C. Mendive, A. Vidal, Mater. Sci. Eng. A-375-377 (2004) 1196–1200.
[7] F. Audebert, B. Idzikowski, P. Svec, M. Miglierini (Eds.), Properties and Applications of Nano-crystalline Alloys from Amorphous Precursors, Nato Science Series II: Mathematics, Physics and Chemistry, 184, Kluwer Acad. Publishers, Dordrecht, 2005, pp. 301–312.
[8] M. Galano, F. Audebert, B. Cantor, I.C. Stone, Mater. Sci. Eng. A 375–377 (2004) 1206–1211.
[9] M. Galano, F. Audebert, I.C. Stone, B. Cantor, Philos. Mag. Lett. 88 (2008) 269–278.
[10] M. Galano, F. Audebert, I.C. Stone, B. Cantor, Acta Mater. 57 (2009) 5107–5119.
[11] M. Galano, F. Audebert, A. García Escorial, I.C. Stone, B. Cantor, Acta Mater. 57-17 (2009) 5120–5130.
[12] M. Galano, F. Audebert, A. García Escorial, I.C. Stone, B. Cantor, J. Alloys Comp. 495 (2010) 372–376.
[13] F. Audebert, M. Galano, C. Triveño Rios, H. Kasama, M. Peres, C. Kiminami, W.J. Botta, C. Bolfarini, J. Alloys Comp. 577 (2013) 650–657.
[14] C.L.H. Thieme, S. Pourrahimi, S. Foner, Scripta Metall. Mater. 28 (1993) 913–918.
[15] I.S. Ahn, S.S. Kim, M.W. Park, K.M. Lee, J. Mater. Sci. Lett. 19 (2000) 2015–2018.
[16] L.Q. Chena, N. Kanetake, Mater. Sci. Eng. A 367 (2004) 295–300.
[17] G. Shiflet, Y. He, S. Poon, Scripta Metall. 22 (1988) 1661–1664.
[18] A. Inoue, K. Othera, A. Tsai, T. Masumoto, Jpn. J. Appl. Phys. 27–3 (1988) L280–L282.
[19] A. Inoue, Prog. Mater. Sci. 43 (1998) 365–520.
[20] D. Bechet, G. Regazzoni, Mater. Sci. Eng. A-134 (1991) 1120–1124.
[21] R. Dunlap, K. Dini, Can. J. Phys. 63 (1985) 1267–1269.
[22] E.S.R. Gopal, S. Baranidharan, J.A. Sekhar, Mater. Sci. Eng. 99 (1988) 413–416.
[23] F. Audebert, B. Arcondo, D. Rodríguez, H. Sirkin, J. Metast. Nanocryst. Mater. 10 (2001) 155–160.
[24] D. Farkas, <http://www.ims.uconn.edu/centers/simul/pot/fefarkas.pot>.
[25] M.S. Daw, M.L. Baskes, Phys. Rev. B 29 (1984) 6443–6453.
[26] F. Saporiti, F. Audebert, S. Gabbanelli, J. Metast. Nanocryst. Mater. 20–21 (2004) 629–634.
[27] Y. Waseda (Ed.), The Structure of Non-Crystalline Materials, McGraw-Hill, USA, 1980.
[28] E. Akiyama, H. Habazaki, A. Kawashima, K. Asami, I.L. Hashimoto, Mater. Sci. Eng. A 226/228 (1997) 920–924.
[29] H. Yoshioka, Q. Yan, H. Habazaki, A. Kawashima, K. Asami, K. Hashimoto, Corros. Sci. 31 (1990) 349–354.
[30] A.N. Mansour, C.A. Melendres, M. Pankuch, S.J. Poon, Y. He, G.J. Shiflet, Surf. Sci. Spectra 2 (1993) 184–194.
[31] A. Mansour, C. Melendres, J. Electrochem. Soc. 142–6 (1995) 1961–1968.
[32] J.E. Sweitzer, G.J. Shiflet, John R. Scully, Electrochim. Acta 48 (2003) 1223–1234.
[33] A.M. Lucente, J.R. Scully, J. Electrochem. Soc. 155–5 (2008) C234–C243.
[34] G.H. Li, W.M. Wang, H.J. Ma, R. Lia, Z.H. Zhang, Y.C. Niu, D.J. Qu, Mater. Chem. Phys. 125 (2011) 136–142.
[35] N.R. Tailleart, R. Huang, T. Aburada, D.J. Horton, J.R. Scully, Corros. Sci. 59 (2012) 238–248.
[36] J. Galvele, S. De Micheli, Corros. Sci. 10 (1970) 795–807.
[37] D. Nelson, Phys. Rev. B 28–10 (1983) 5515–5535.
[38] D. Herlach, D. Holland-Moritz, P. Galenko (Eds.), Metastable Solids from Undercooled Melts, Pergamon Materials Series, Elsevier, Germany, 2007.